Astrophys Space Sci (2006) 305:37–47
DOI 10.1007/s10509-006-9039-6

ORIGINAL ARTICLE

Geoeffective Analysis of CMEs Under Current Sheet Magnetic Coordinates

Xueshang Feng · Xinhua Zhao

Received: 9 September 2005 / Accepted: 16 January 2006

Abstract Using 100 CME–ICME events during 1997.01–2002.11, based on the eruptive source locations of CMEs and solar magnetic field observations at the photosphere, a current sheet magnetic coordinate (CMC) system is established in order to statistically study the characteristics of the CME–ICME events and the corresponding geomagnetic storm intensity. The transit times of CMEs from the Sun to the Earth are also investigated, by taking into account of the angle between the CME eruption normal (defined as the vector from the Sun center to the CME eruption source) and the Sun-Earth line. Our preliminary conclusions are: 1. The distribution of the CME sources in our CMC system is obviously different from that in the ordinary heliographic coordinate system. The sources of CMEs are mainly centralized near the heliospheric current sheet (HCS), and the number of events decreases with the increment of the angular distance from the CME source to the HCS on the solar surface; 2. A large portion of the total events belong to the same–side events (referring to the CME source located on the same side of the HCS as the Earth), while only a small portion belong to the opposite–side events (the CME source located on the opposite side of the HCS as the Earth). 3. The intense geomagnetic storms are usually induced by the same–side events, while the opposite side events are commonly associated with relatively weak geomagnetic storms; 4. The angle between the CME normal and the Sun–Earth line is used to estimate the transit time of the CME in order to reflect the influence of propagation characteristic of the CME along the Sun–Earth direction. With our new prediction method in context of the CMC coordinate, the averaged absolute error for these 100 events is 10.33 hours and the resulting relative error is not larger than 30% for 91% of all the events.

Keywords Coronal mass ejections · Current sheet magnetic coordinate · Geomagnetic storm intensity · Transit time · Prediction method

X. Feng (✉) · X. Zhao
SIGMA Weather Group, State Key Laboratory for Space Weather Center for Space Science and Applied Research, Chinese Academy of Sciences, P. O. Box 8701, Beijing, 100080, China
e-mail: fengx@spaceweather.ac.cn

X. Zhao
Graduate University of the Chinese Academy of Sciences, Beijing 100049, China

1. Introduction

Coronal mass ejections (CMEs), which refer to large–scale magnetized plasma structures that erupt from the sun and are transported into the heliosphere, are a kind of eruptive phenomena in solar atmosphere usually associated with flares or eruptive prominences. They are episodic expulsions of mass and magnetic field from the solar corona into the interplanetary medium, producing significant perturbations in the solar wind and the geomagnetic environment. These huge ejected plasmoids may have masses of the order of a few 10^{15} g and likely liberate energies between $10^{30} - 10^{32}$ ergs. CMEs were first identified in data obtained with space-borne coronagraphs in the 70's of last century (MacQueen et al., 1974; Gosling et al., 1974; MacQueen et al., 1980; Sheeley, 1980). In earlier days, CME was believed to correlate well with the occurrence of a geomagnetic storm (Burlaga et al., 1981; Wilson et al., 1984) and it was thought that solar flares–generated interplanetary shocks were responsible for geomagnetic storms. However, later evidences show that CMEs are major sources for non–recurrent geomagnetic storms (Sheeley, 1985; Gosling, 1991, 1993).

Since then they have captured the attention of both the solar and the geomagnetic communities. Several excellent review papers have been written in the last years (Crooker, Joselyn and Feynman, 1997; Hundhausen, 1999; Pick et al., 1999; Forbes, 2000; Klimchuk, 2000; Webb, 2000; Hudson and Cliver, 2001). One of the challenging works on theoretical and observational aspects of CMEs is the "Q&A" review by Cliver and Hudson (2002). Numerical modeling of CMEs has always been a hot topic along with the development of high performance computing. Linker et al. (2003) reviewed some of the past and present concepts that influence the development of models of coronal mass ejections, both for CME initiation and CME evolution and propagation in the solar wind. Also Riley et al. (2004) summarized their recent advances in modeling the properties and evolution of CMEs in the solar wind.

Currently, the exact causes and mechanism of CME are not well understood and debated in the scientific community. The earth directed coronal mass ejections are often correlated with intense geomagnetic storms, interplanetary shocks and energetic particle events, which disrupt radio communications, cause surges in power grids and damage satellites. Understanding these events and developing predictive capabilities is a very important scientific challenge. Especially, how to predict the CME related geomagnetic storm intensity and the Sun-Earth transit time of the CME become two important aspects in space weather forecast.

There are a huge of works on CMEs such that it is difficult to exhaust a review on CMEs by giving a long list of publications. In what follows we focus our attention on our interest by only mentioning as few related work as needed in the following content.

Wei et al. (1990, 1991) statistically studied 277 flare–shock events and found that the existence of the HCS might have great influence on the propagation of solar transient disturbances in interplanetary space and the corresponding geomagnetic disturbances intensity; The transient disturbances caused by solar activities would deflect towards the HCS in their travelling to the Earth regardless of the discrimination that the solar sources are located on the northern or southern hemisphere. Wei and Dryer (1991) analyzed 149 flare-shock wave events based on interplanetary scintillation (IPS) observational data and found the fastest propagation directions tend toward the HCS near 1AU. Similar results were also found by later studies (Dryer, 1994; Odstrcil et al., 1996; Smith et al., 1998). Therefore, we can see that the HCS near the Sun is very important in studying the propagation of solar transient disturbances and their related geomagnetic storms. Following the idea of Wei et al. (1990, 1991), in order to carry out geoeffective analysis of CMEs, a current sheet magnetic coordinate (CMC) system is established and used to analyze 100 CME-ICME events during 1997.01–2002.11.

This paper is organized as follows. In Section 2, the establishment of CMC system is presented. In Section 3, 100 CME-ICME events are statistically studied under this coordinate system to draw the conclusion that the geomagnetic disturbances caused by CMEs tend to have the "same side-opposite side effect". In Section 4, a new method is given to predict when the ICME arrives at the Earth after considering the CME normal direction relative to the Sun-Earth line in context of the CMC system. Conclusions and discussions are made in Section 5.

2. Current sheet magnetic coordinate system

2.1. Establishment of the CMC system

This subsection is devoted to the establishment of the CMC system. In the same way as done by Wei et al. (1990; 1991), the erupting location of the CME and the large–scale shape of the HCS near the Sun are used here. When a CME erupts, it leaves behind hot post–eruption arcades or flare loops that mark the source location of the eruption on the surface of the Sun. This coordinate to be defined is a rectangular coordinate system whose origin is at the center **O** of the Sun as shown in Fig. 1(a). The curved surface labelled as **HCS** in Fig. 1(a) is the real heliospheric current sheet. **S** is the source location of the CME at 2.5 solar radii. The direction **ON**, defined as the normal of the CME eruption, is the vector from the center of the Sun to the source of the CME. And the point **P**, located on the HCS, is the foot of the perpendicular from the point **S** onto the **HCS**. The vector **OP** is defined as the X axis. We select a local segment of the real HCS near the foot **P** (shadowed region) and extend it to a plane XOY that passes through the center of the Sun. We call this plane the "ideal HCS" labelled as **ICS** in Fig. 1(a). The X axis and the CME normal **ON** constitute the plane XOZ, which is considered to be the symmetrical plane for coronal mass ejections. These two orthogonal planes constitute the coordinate system in this paper, named Current sheet Magnetic Coordinate (CMC) system. Obviously, the basis vectors X, Y, and Z complete a right-handed triad. Besides x, y and z, we can also define the latitude λ and longitude η to describe the position of the Earth in this coordinate. Here, λ stands for the angle between the Sun–Earth line and its projection on the plane XOY. That is to say, λ stands for the angle between the Sun-Earth line and the HCS. η stands for the angle from the X axis to the projection of the Sun–Earth line on the plane XOY. These two angles are defined to be perpendicular to each other, i.e.,

$$\lambda = \arctan\left(\frac{z}{\sqrt{x^2+y^2}}\right), \quad \eta = \arctan\left(\frac{y}{x}\right)$$

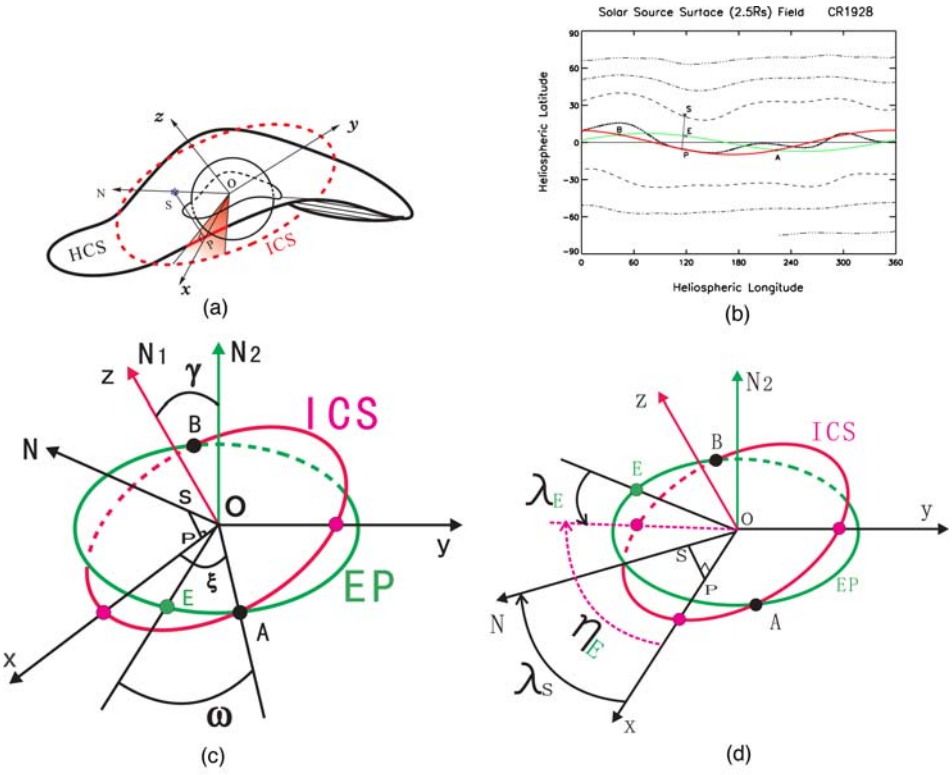

Fig. 1 (a) The 3D sketch map of the CMC system, (b) Its spread on solar magnetic field synoptic chart, (c) The useful angles in CMC coordinate with ICS and EP, and (d) The coordinates of the Earth and CME source in CMC system. In (a), **O** is the center of the Sun, **S** is the CME erupting source, **N** is the normal of CME, **HCS** stands for the real heliospheric current sheet, **P** is the foot of a perpendicular of **S** on the HCS and **ICS** stands for the ideal HCS. In (b), curve 1 represents the HCS, curve 2 represents the ideal HCS, curve 3 represents the ecliptic plane, **S** and **P** as in (a), **E** is the sub–Earth point at the CME erupting moment, **A** and **B** are points of intersection for the ecliptic plane and the ideal HCS. In (c), angles γ, ξ, ω used in CMC are displayed with EP standing for the ecliptic plane. N_1 and N_2 are normals of the ICS plane and ecliptic plane, respectively. In (d), the latitude λ_E and the longitude η_E for the Earth and λ_S for the CME source are labeled

One thing to be stressed here is that the local HCS near CME source is outspread here to a plane (called ideal HCS) and the established coordinate system is static. However, the real HCS is very complex and it rotates with the Sun with a period of about 27 days. The theoretical basis for these approximations is as follows: It takes the CME only 5–9 hours to pass through the inner heliosphere (18–20Rs), where magnetic field controls the motion of plasma. Then the real HCS rotates with the angle of only about 3°–5° within this short interval. The influence of magnetic field on plasma motion decreases rapidly when the CME propagates into the heliosphere beyond the Alfvénic point. Thus the effect of the HCS beyond the Alfvénic point on the CME propagation could be regarded as inessential and thus the ideal HCS can be taken as an approximation to the real HCS. Furthermore, as **P** is the foot of the perpendicular of the CME source on the real HCS, the latitude of the CME source in CMC (see Subsection 2.3) represents the true angle from the CME normal to the real HCS.

2.2. The coordinates of the earth and the CME source in the CMC system

In this subsection it is shown how the CMC system works for an event. As an example, Fig. 1(b) demonstrates the spread of the CMC system on the contour of solar source surface magnetic field for CR 1928 located at 2.5 solar radii from the Wilcox Solar Observatory. The neutral line in this chart is the HCS at 2.5Rs curve 1. There was a CME event erupting from N22E01 at 11:26 UT on 23 October 1997. In Fig. 1(b) we find the point **S** for the source location of this CME event according to the erupting location, the erupting date and time. **P** is the foot of the perpendicular from the point **S** onto the HCS. Curve 2 stands for the ideal HCS that is outspread by the local real HCS centered about the foot **P. E** stands for the location of the Earth at the erupting moment and curve 3 stands for the ecliptic plane. **A** and **B** are points of intersection for the ecliptic plane and the ideal HCS.

The coordinates of the Earth in the CMC system can be derived from three angles, i.e., γ, ξ and ω. Here, γ denotes the angle between the ecliptic plane and the ideal HCS (or the angle between their normals). ξ denotes the angle between **OP** and **OA**. Denote ω the angle between **OE** and **OA.** Then we have

$$\gamma = \arccos\left(\frac{n_{1x}n_{2x} + n_{1y}n_{2y} + n_{1z}n_{2z}}{\sqrt{n_{1x}^2 + n_{1y}^2 + n_{1z}^2}\sqrt{n_{2x}^2 + n_{2y}^2 + n_{2z}^2}}\right)$$
$$\xi = \arccos(\cos(\phi_A - \phi_P)\cos(\psi_A - \psi_P)),$$
$$\omega = \arccos(\cos(\phi_A - \phi_E)\cos(\psi_A - \psi_E))$$

where $\mathbf{N}_1 = (n_{1x}, n_{1y}, n_{1z})$ and $\mathbf{N}_2 = (n_{2x}, n_{2y}, n_{2z})$ denote the normals of the ideal HCS and the ecliptic plane in the solar equator coordinate system respectively (See Fig. 1(c)). ϕ_A, ψ_A, ϕ_P, ψ_P and ϕ_E, ψ_E denote the longitudes and latitudes of **A**, **P** and **E** as shown in Fig. 1(b). If the values of γ, ξ and ω are known, then we can get the coordinates of the Earth in the CMC system:

$$x_E = \cos(\xi)\cos(\omega) + \sin(\xi)\cos(\gamma)\sin(\omega) \quad (1a)$$

$$y_E = -\sin(\xi)\cos(\omega) + \cos(\xi)\cos(\gamma)\sin(\omega) \quad (1b)$$

$$z_E = -\sin(\gamma)\sin(\omega) \quad (1c)$$

where x_E, y_E and z_E are in units of AU. Then,

$$\lambda_E = \arctan\frac{z_E}{\sqrt{x_E^2 + y_E^2}}, \quad \eta_E = \arctan\frac{y_E}{x_E} \quad (2)$$

While the coordinates of the CME source in the CMC system (see Fig. 1(d)) are

$$\lambda_S = \arccos(\cos(\phi_S - \phi_P)\cos(\psi_S - \psi_P)), \quad \eta_S = 0 \quad (3)$$

where ϕ_S, ψ_S and ϕ_p, ψ_P denote the longitudes and latitudes of **S** and **P** in Fig. 1(b). We can see from Fig. 1(a) that the z axis of the CMC system is defined to lie on the same side of the ideal HCS as the CME source. Then λ_S computed from our formulas is always positive for CMEs that erupt from either north hemisphere or south hemisphere. While λ_E is positive for the same side events (abbreviated to "the SS events" in the following for convenience) and negative for the opposite side events (abbreviated to "the OS events" in the following). Therefore, we can judge a CME to be the SS or OS event only by the sign of λ_E in the CMC system (see Fig. 1(d)). In context of this coordinate system mentioned above, we can calculate the parameters for the CME event erupting at 11:26 UT on 23 October 1997: $\lambda_S = 27.5^\circ$, $\eta_S = 0^\circ$, $\lambda_E = 11.0^\circ$, $\eta_E = 3.6^\circ$ We draw the conclusion that this CME event erupted from the same side of the HCS as the Earth from the positiveness of λ_E. Fig. 1(b) also displays this fact.

3. The same side-opposite side effect for CMEs and their geoeffectiveness

100 CME–ICME events during 1997.01–2002.11 are collected for this analysis, which contains the following observations: the time of its first appearance in LASCO/C2, projected speed, the erupting location, the arrival time of the corresponding ICME at the near Earth spacecraft and the related geomagnetic storm intensity. These parameters are taken from the recognized results in the published papers (Webb et al., 2000; Gopalswamy et al., 2001; Cane and Richardson, 2003; Manoharan et al., 2004; Michalek et al., 2003) together with these websites http://cdaw.gsfc.nasa.gov/CME_list/index.html, http://www.gi.alaska.edu/pipermail //gse-ff/, ftp://ftp.ngdc.noaa.gov/STP/GEOMAGNETIC_DATA/ INDICES/ DST/, http://www. ngdc.noaa.gov/ stp/SOLAR/ ftp-solarflares.html. From our choice are excluded those events whose erupting locations and/or the arrival time of the associated ICME are recognized to be evidently different in different papers and also the events that lack the clear locations of the CME eruption. As for each event in our samples, we draw the solar magnetic field synoptic chart of the Carrington Rotation during which the CME erupted according to the observations of the Wilcox Solar Observatory (http://quake.stanford.edu/ wso/coronal.html), establish the CMC system and then calculate the coordinates of the Earth and the CME erupting source in this coordinate. These information for 100 CMEs in this coordinate system are used for the following analysis.

3.1. The distribution characteristics for the CME sources

In order to demonstrate the difference between the CMC system and the commonly used heliographic coordinate system in studying CMEs, we analyze the distribution characteristics of these 100 events in these two coordinate systems, respectively. Figure 2 gives the frequency distributions of the heliographic latitudes and heliographic longitudes (here referring to longitudinal displacement from central meridian) for these CME source locations. From this figure we can see that the latitude distribution of the CME sources presents a "double-peak" structure. That is to say, CMEs mainly erupt from the middle and low latitude regions with the maximum numbers located within $\pm(10^\circ - 30^\circ)$, while few CMEs erupt from high latitude regions. As for the longitude distribution, most are located near the central meridian as we expect. It is shown that the distribution characteristics of the CME sources in the heliographic coordinate for our 100 events are consistent with

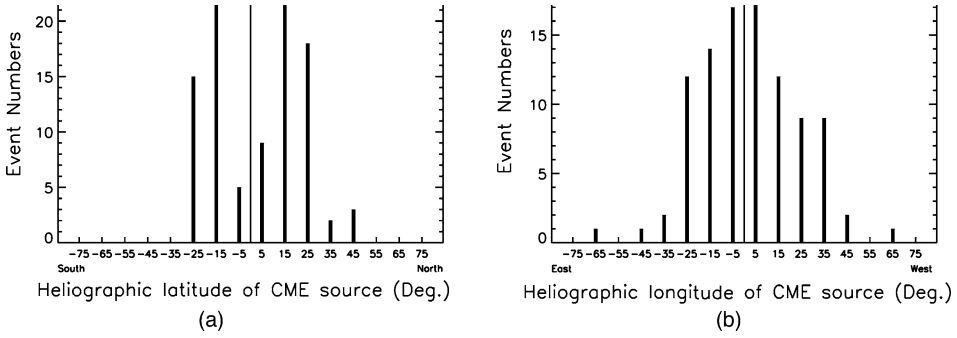

Fig. 2 The frequency distribution of heliographic latitudes (a) and heliographic longitudes (b) of the CME sources. The event numbers are summed over 10 degree bins, and in (b) the longitude refers to longitudinal displacement from central meridian

the results of related studies (Cane, Richardson and St. Cyr, 2000; Wang et al., 2002; Manoharan et al., 2004; Srivastava and Venkatakrishnan, 2004; Shrivastava and Singh, 2005).

As a contrast, Fig. 3 exhibits a distribution of the CME sources in the CMC coordinate. In Fig. 3(a), the angle from CME normal to the HCS is calculated from formula (3) and its sign is defined as follows: if the ideal HCS lies to the south of the CME source, then the value is positive and otherwise it is negative. This definition is in agreement with the solar equatorial coordinate system. Now, the "double-peak" distribution in Fig. 2 is replaced by the approximate Gaussian distribution in Fig. 3(a). The distribution is symmetrical relative to the HCS with the maximum numbers located near the HCS. This implies that CMEs originate most frequently near the heliospheric current sheet (HCS) which is sandwiched between coronal holes having opposite magnetic polarity. This findings reconfirm the earlier results shown by Crooker et al. (1993) and developed further by Kahler et al. (1999) and Zhao and Webb (2003).

Figure 3(b) is given based on the same data as Fig. 3(a) but considering the same side-opposite side effect. In Fig. 3(b) the angle from CME normal to the HCS is defined to be positive when the Earth and the source location of the CME lie on the same side of the HCS (the SS event) and negative when the Earth and the source location of the CME lie on the opposite side of the HCS (the OS event). It is evident from this figure that the number of the SS events is larger than that of the OS events ($74 > 26$). Furthermore, the SS events occupy a broader latitude extent. Comparing Fig. 2 with Fig. 3, we can draw the conclusion that the CMC system has more advantages in depicting the relative positions between the CME eruption source, the Earth and the HCS than the heliographic coordinate system owing to the fact that the former take the HCS (ideal) as the reference plane, while the latter take the solar equator as the reference plane.

In order to further display the influence of the HCS on the propagation and arrival of CME-ICME from the Sun to the Earth, we investigate the position of the Earth relative to the HCS in the same way and the distribution of the angles between the Sun-Earth line and the HCS for these 100 events is shown in Fig. 4. In Fig. 4(a), the angle is given by $|\lambda_E|$ in the CMC system but defined to be positive when the HCS lies to the south of the Earth and negative on the contrary. It is easily seen that the positions of the Earth are nearly symmetrical about the HCS. That is to say, the Earth, as the detector of the ICMEs, has equivalent opportunities to appear on both southern and northern side of the HCS. Also, more ICMEs are detected when the Earth is located near the HCS. Fig. 4(b) gives the same plot as Fig. 4(a) but considering the same side-opposite side effect as a contrast, i.e., using λ_E in the CMC system. There also follows that there is a distinct asymmetry in the distribution. On one hand, there are more SS events than OS events. On the other hand, this angle between the Sun-Earth line and the HCS can exceed 70° for some CMEs of the SS events; however, it does not exceeds 30° for the OS events under investigation. Considering the thickness of the real HCS, we could say that for our unbiased sample of 100 geoeffective CME-ICME events, those events with their eruptive sources lying on the same side of the HCS and/or the Earth being near the HCS have been found to be rich, and no ICME among these 100 events was observed when the Earth is located on the opposite side of as well as far away from the HCS. The reasons causing these statistical results could be complicated and perplexing, but one possible explanation is that as the HCS is a surface that separates regions of the magnetic field with different polarities and the magnetic field-frozen condition is satisfied in interplanetary space, this may imply that the CME-ICME has difficulty to traverse the HCS in its passage to the Earth.

3.2. The distribution characteristics for the corresponding geomagnetic storm intensity

The plot of the geomagnetic storm intensity (Dst_{min}) versus the angles between the HCS and the Sun-Earth line is given in Fig. 5. In Fig. 5(a) the x-coordinate is the same as that of Fig. 4(a). Fig. 5(a) tells us that the distribution of Dst is approximately symmetrical relative to the HCS: on one hand, there are more events appearing when the Earth is located near the HCS, especially more intense geomagnetic storms; on the other hand, there is no distinct difference for both cases whenever the Earth lies on the southern and northern side of the HCS.

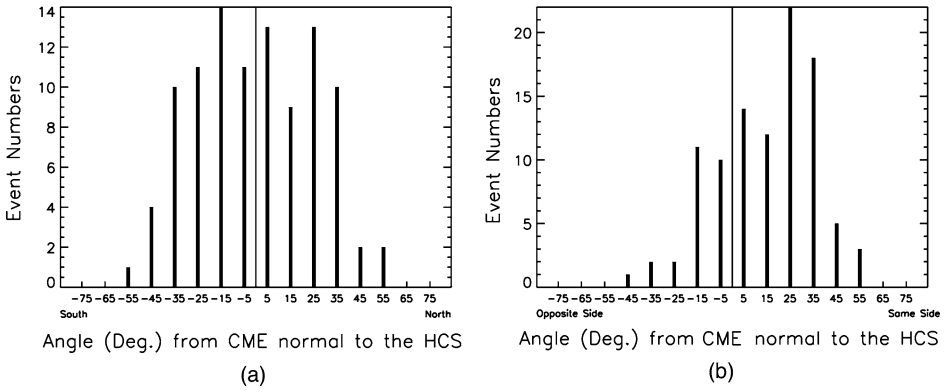

Fig. 3 The frequency distribution of the CME sources in the CMC coordinate (a) without the same side-opposite side effect and (b) with the same side-opposite side effect

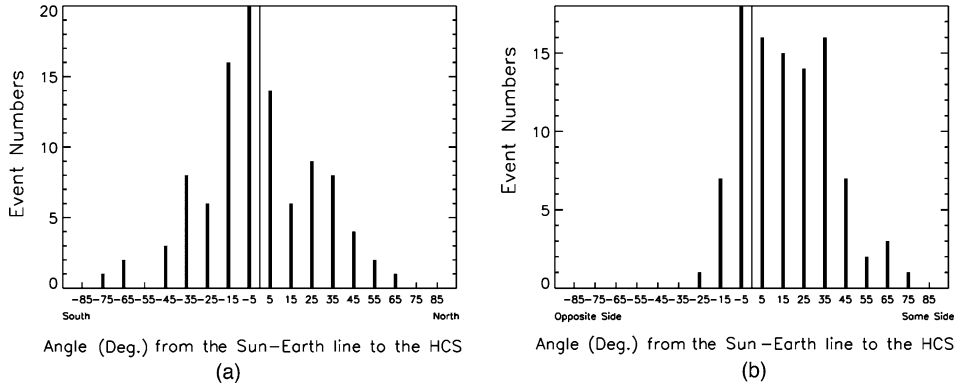

Fig. 4 The frequency distribution of the angles between the Sun-Earth line and the HCS (a) without the same side-opposite side effect and (b) with the same side-opposite side effect

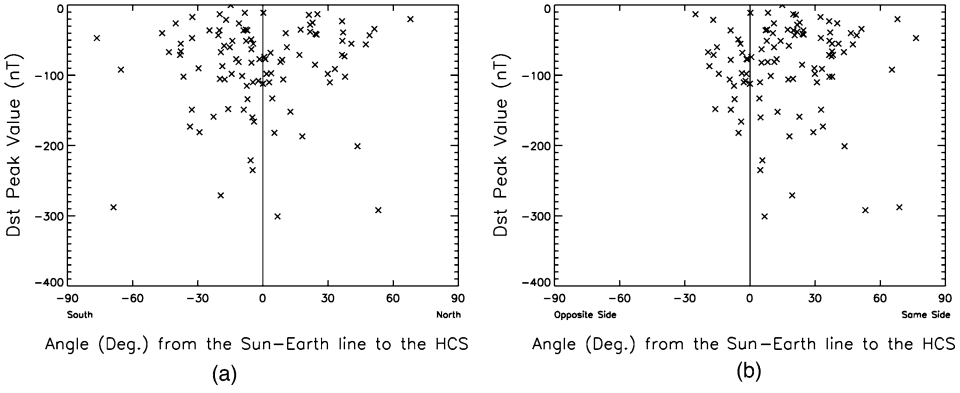

Fig. 5 The geomagnetic storm intensity plotted against the angles between the Sun-Earth line and the HCS. (a) without the same side-opposite side effect and (b) with the same side-opposite side effect

Figure 5(b) gives the geomagnetic storm intensity plotted against λ_E in the CMC system, considering the same side-opposite side effect. From this figure we can see that: (1) There is a distinct asymmetry in the distribution of the events. There are 74 SS events among the total 100 events, while there are merely 26 OS events as mentioned in section 3.1; (2) For 68 moderate geomagnetic storms ($Dst_{min} < -50$ nT), 46 of them are the SS events and 22 of them are the OS events. The event percentage for the SS and OS events are respectively 68%, 32%; (3) For 32 intense geomagnetic storms ($Dst_{min} < -100$ nT), 22 of them are the SS events (occupying 69% of the total) and 10 are the OS events (occupying 31% of the total); (4) For 15 geomagnetic storms with $Dst_{min} < -150$ nT, 13 of them are the SS events (87% of the total) and only 2 of them are the OS events (13% of the total); (5) All the geomagnetic storms with $Dst_{min} < -200$ nT appear as the SS events. It can be seen that the percentage of the SS events increases with the increment of geomagnetic storm intensity, while the percentage of the OS events decreases with that, as shown by Fig. 6. This means the intense geomagnetic storms are apt to be caused by the SS events, and the OS events are commonly associated with relatively weak geomagnetic storms.

The above results indicate that there exists a so-called "same side-opposite side effect" in the geomagnetic disturbances caused by CMEs: for an unbiased sample of 100 CME-ICME events that have observable effects at 1AU, the event frequency of the SS events is statistically higher than

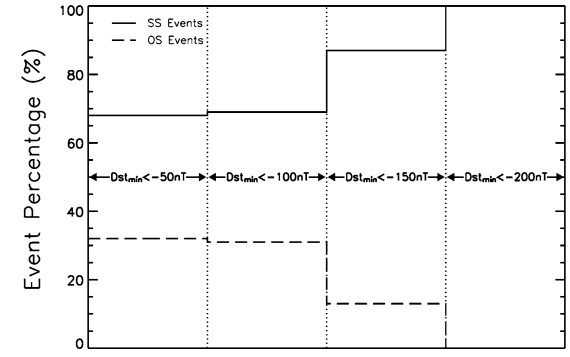

Fig. 6 The distribution of event percentage for different ranges of geomagnetic storm intensity. The solid and dashed line represent that of the same side and opposite side events respectively

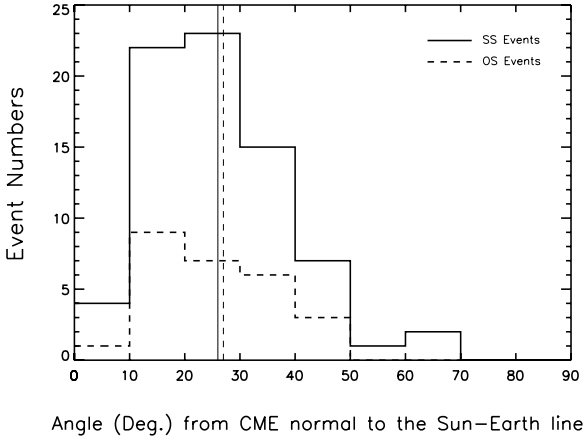

Fig. 7 The frequency distribution of angles between the CME normal and the Sun-Earth line. The solid and dashed line represent the same side and opposite side events respectively

that of the OS events; the intense geomagnetic storms are usually caused by the SS events; the existence of the HCS may have important influence on the propagation–arrival of CME-ICMEs and their induced geomagnetic disturbances. The possible "impeding" effect of the HCS on the transpropagation of CMEs mentioned above can explain, at least partially, the above statistical results. These results again reconfirm the observational results obtained by Wei et al. (1990, 1991) for solar flares.

It should be mentioned that the angle between CME normal and the Sun-Earth contribute little to the classification of same side-opposite side. Fig. 7 gives the distribution of these angles for the 100 CME-ICME events. The thick solid and dashed line denote the SS and OS events respectively. The frequency distributions for the SS and OS events are similar to a great extent and their mean values of the angles are nearly equal as shown by the vertical solid and dashed line. Therefore, these angles make no contribution to our statistical results, and the "same side-opposite side effect" is mainly caused by the existence of the HCS.

4. The prediction of CME's transit time

As the arrival near the Earth of the solar transient disturbances usually implies the onset of the geomagnetic storms, the arrival time prediction has been regarded as an important aspect of space weather objectives. Roughly speaking, there are two kinds of models for the prediction of the solar disturbances' arrival at the Earth: (I) physics-based shock propagation models and (II) empirical CME propagation models. Among the shock propagation models, STOA (Dryer and Smart, 1984; Smart and Shea, 1985), STOA-2 (Moon et al., 2002), ISPM (Smith and Dryer, 1990, 1995) and HAFv.2 (Hakamada and Akasofu, 1982; Fry et al., 2001) are commonly used models. The STOA is based on the theoretical concept of self-similar blast waves modified by the piston-driven idea, while the STOA-2 adopts a linear relationship between the initial coronal shock wave velocity and its deceleration exponent for improvements. The ISPM relies on a 2.5D MHD parametric study of numerically simulated shocks and it assumes that the net energy ejected into the solar wind by a solar source together with the source's location determine the transit time to 1 AU of the shock. The HAFv.2 is a "modified kinematic" solar wind model that can provide a global picture of multiple and interacting shocks propagating into nonuniform, stream-stream interacting solar wind flows. By combining the observations of solar activity, interplanetary scintillation and geomagnetic disturbance observations together with the dynamics of solar wind storm propagation and fuzzy mathematics, Wei and Cai (1990) and Wei et al. (2002, 2003) gave a new "ISF" prediction method for geomagnetic disturbances caused by solar wind storms blowing to the Earth.

Our current knowledge about CMEs mainly comes from two spatial domains: the near-Sun region remote-sensing by coronagraphs and the near-Earth space where in situ observations are made by spacecrafts. Therefore, people usually rely on empirical models to predict the 1AU arrival time of CMEs. Brueckner, Delaboudiniere and Howard (1998) had ever concluded that the travel time of most ICMEs from the Sun to the Earth always amounts to about 80 hours based on eight CME events, where the travel time was measured from the first appearance in C2 images to the beginning of the maximum Kp index of the associated geomagnetic storm. This "80 hours rule", as the simplest prediction tool, seems to work well in many cases, especially near solar activity minimum. Wang, Ye and Wang (2002) studied 15 events that were associated with severe storms ($K_p > 7$) and found that the transit time of the CMEs can be predicted by this formula

$$T = 27.98 + 2.11 \times 10^4 / V_p$$

where V_p(km/s) is the CME projected speed and T (hours) is the transit time of the CME defined as the interval from

CME's first appearance in C2 to to the beginning of the maximum Kp index of the associated geomagnetic storm. Srivastava and Venkatakrishnan (2004) determined an empirical relation between the transit time and the initial speed from 64 CME events

$$T = 86.9 - 0.026V_p$$

Here T (hours) is the difference in the timings of the start of the CME and the time of the onset of the geomagnetic storm marked by the decrease in Dst values, while V_p (km/s) is also the CME projected speed. Schwenn et al. (2005) studied the relationship between the lateral expansion speed of the CME and its travel time to the Earth. They found that the fit function

$$T = 203 - 20.77\ln(V_{\exp})$$

gives the least-square errors for the 75 usable cases of unique CME-shock events, where T is defined by the CME's first appearance in C2 images and the shock arrival at 1AU in units of hours, and $V_{\exp}$ is the halo expansion speed in km/s.

The ECA (Empirical CME Arrival) model was developed by Gopalswamy et al. (2000, 2001) for the prediction of the CME arrival. In this model CMEs are believed to undergo an interplanetary acceleration speed a that depends linearly on the CME initial speed u until propagating to the cessation distance d_1

$$a = \alpha - \beta u, \quad S = ut + at^2/2$$

with α and β positive constants. CMEs propagate freely beyond this cessation distance to 1AU $d_2 = 1AU - d_1$ Then the arrival time of the ICME at the Earth can be expressed as $t = t_1 + t_2$, where

$$t_1 = [(u^2 + 2ad_1)^{0.5} - u]/a, \quad t_2 = d_2/(u^2 + 2ad_1)^{0.5}$$

Gopalswamy et al. (2001) studied 47 CME-ICME events during 1996.12–2000.7 and found $\alpha = 2.193$, $\beta = 0.0054$ while the typical value of d_1 is 0.76 AU. The mean absolute error of this model is 10.7 hours for these 47 events. It must be pointed out that different authors considered different samples of CME events and they adopted different definitions of the transit times of the CMEs, then the formulas they provided are also discrepant. But all these studies showed that the transit time of the CME depends on its initial speed to a great extent. Unfortunately, what is available now is the projected speed of the CME's space speed on the sky plane (perpendicular to the Sun-Earth line) near the Sun, and this speed can't stand for the propagation speed of the CME to the Earth. However, just as Gopalswamy et al. (2001) pointed out, the projection effects may be somehow compensated for by the initial expansion of the CME. Then the sky plane speed seems to be a reasonable representation of the CME initial speed. An innovative analytical method has been derived by Zhao et al., (2002) and Xie, Ofman and Lawrence (2004) to determine the angular width and central position angle of a cone model CME and the CME transit time was estimated by using actual radial speeds for several cases.

Except for its initial speed, the transit time of the CME also depends on the propagation process of the ICME in interplanetary space and the direction of the CME eruption. MacQueen, Hundhausen and Conover (1986) pointed out that the propagation of CME transients in the inner corona is "tilted" toward the solar equator and this may be the results of the nonradial force acting upon the CME material by the background coronal magnetic and flow patterns. Since the HCS is a characteristic reference surface for the organization of solar wind plasma, the studies of the influence of the HCS on the propagation of the solar disturbances in interplanetary space have attracted a lot of attention. Wei and Dryer (1991) analyzed 149 flare-shock wave events based on interplanetary scintillation (IPS) observational data and found that the flare-associated shock waves, deviating from the flare normal, tend to propagate toward the low latitude region with respect to the HCS. Also, the fastest propagation directions tend toward the heliospheric current sheet near 1AU and the meridional shape of the typical shock wave is roughly symmetrical relative to the heliospheric current sheet. Smith, Odstrcil and Dryer (1998) performed a 2.5-dimensional MHD parametric study to explore the effect of the HCS and HPS (heliospheric plasma sheet) on the shock propagation and draw the conclusion that both the shock travel time and the shock properties at 1 AU are affected when the shock crosses the HPS in which the HCS is embedded. In the prediction of the arrival of shocks, both STOA (Dryer and Smart, 1984; Smart and Shea, 1985) and ISPM (Smith and Dryer, 1990, 1995) model consider the flare source as one of the parameters that determine the arrival time of the shock.

All these studies mentioned above, such as the study of considering the nonradial force acting upon the CME material by the background coronal magnetic and flow patterns, the result that the fastest propagation directions of flare-associated shock waves tend toward the heliospheric current sheet near 1AU, combined with our conclusion about the influence of the HCS on the propagation of the CME-ICME, imply that the helisohperic current sheet can affect the CME's moving in interplanetary space. But, how to quantify this effect is a difficult task in our present knowledge since the physical mechanism for CME's formation, the fundamental process of its propagation in interplanetary space is unclear. After the establishment of the CMC, the angle between the CME normal, the Sun-Earth line and the HCS could provide us a candidate for quantifying such effect. And in our CMC coordinate it is natural and convenient for

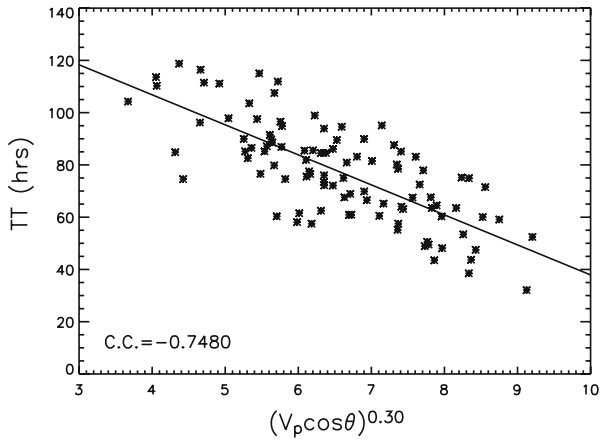

Fig. 8 The scatter plot of the CME transit time (TT) versus $(V_p \cos\theta)^{0.30}$. The solid lines are the linear fitting

us to consider the angle between the solar disturbance (such as CME) normal and the Sun-Earth line. As for the CME, the angle θ from the CME eruption normal (connecting the center **O** of the Sun to the source **S** of the CME) to the Sun-Earth (the detector of the ICME) can be obtained conveniently in our CMC system by $\cos\theta = \cos(\lambda_S - \lambda_E)\cos(\eta_E)$, where $\lambda_S - \lambda_E$ and $0 - \eta_E$ denote the components of θ perpendicular to and parallel to the ideal HCS. Then $V_p \cos\theta$ stands for the propagation speed of the CME in the direction toward the Earth. This consideration motivates us to investigate the correlation between $[V_p \cos\theta]^\beta$ and the transit time (TT), where β is adjustable. In this paper, we define the transit time (TT) of the CME to be the difference in the timings of the first appearance of the CME in the LASCO/C2 coronagraph and the time of the arrival of the corresponding ICME in situ observation at L1 point. Then, it is found that $\beta = 0.30$ gives the maximum correlation of C.C. $= -0.7480$ as displayed in Fig. 8. Up to now we give a new prediction method for the transit time of the CME based on its projected speed and eruption direction relative to the Sun-Earth line:

$$TT = 152.8 - 11.49[V_p \cos\theta]^{0.3} \tag{4}$$

where TT and V_p are in units of hours and km/s, respectively. The applicability range of this formula is $0.4 \leq \cos\theta \leq 1.0$.

Figure 9(a) demonstrates the predicted results $TT_{\rm pre}$ of the transit times for these 100 events in this method and the observational values $TT_{\rm obs}$. Fig. 9(b) shows the computed error of this prediction (observation minus prediction). The mean absolute error of this method is 10.33 hours for these 100 events. The results of the prediction test show the relative errors $\delta TT = \frac{|TT_{\rm obs} - TT_{\rm pre}|}{TT_{\rm obe}} \leq 10\%$ for 45% of all events, $\leq$ 20% for 73%, and only 9% of all events with relative errors $> 30\%$.

5. Conclusions and discussions

Based on the eruptive sources of CMEs and their coronal magnetic environment, a current sheet magnetic coordinate is established in order to study the propagation - arrival of CMEs and their geoeffectiveness. In context of this coordinate, the relative locations between the CME source, the Earth and the HCS at CME erupting time can be investigated conveniently. For the first time, the CME's actual speeds and source locations and their related positions with the HCS are determined quantitatively by using coronagraph data and solar photospheric magnetic field observation. These parameters are critically important in space weather modelling.

100 CME-ICME events during 1997.01–2002.11 are statistically studied to find that (1) CMEs, which have their 1AU counterparts near the Earth, erupt most frequently near the heliospheric current sheet (HCS). The event frequency of the same side (SS) events is obviously higher than that of the opposite side (OS) events after considering the relative positions of the CME source and the Earth with respect to the HCS. And the intense geomagnetic storms are usually caused by the SS events. The HCS might have the "impeding" effect on CME's trans-propagation; (2) the source of CME and its nearby form of the HCS will also affect its arrival time at the Earth.

By the way, based on the projected speed, source location and the angular separation from CME normal to the Sun-Earth direction, in context of the CMC coordinate we arrive at a new prediction method for estimating arrival time. The application of our empirical formula for 100 CME-ICME events shows that the averaged absolute error for these 100 events is 10.33 hours.

While our method produces realistic advances using the actual observation of CMEs such as speed, source location and photospheric magnetic field observation, there are some questions for improvement.

First, the three dimensional structure of the real HCS is very complex, while the CMC is a static coordinate system. In the establishment of the CMC system, we only consider the influence of large-scale solar magnetic structures on interplanetary disturbances, and neglect factors such as the rotation of the Sun and the influence of other segments of the HCS far away from the CME eruption region. Therefore our model is an approximation to a certain extent.

Second, the prediction of interplanetary magnetic field Bz in ICME, another important constraint on geoeffective CMEs, is not addressed in the present study.

Finally, the accuracy of CME transit time prediction relies on the accuracy of CME actual speeds, accelerations and realistic solar wind ambient. Currently, apparent speeds and accelerations of CMEs can only be measured within 30 Rs (field of view of LASCO/C3). Theoretical and numerical studies on the interaction between CMEs and the solar wind

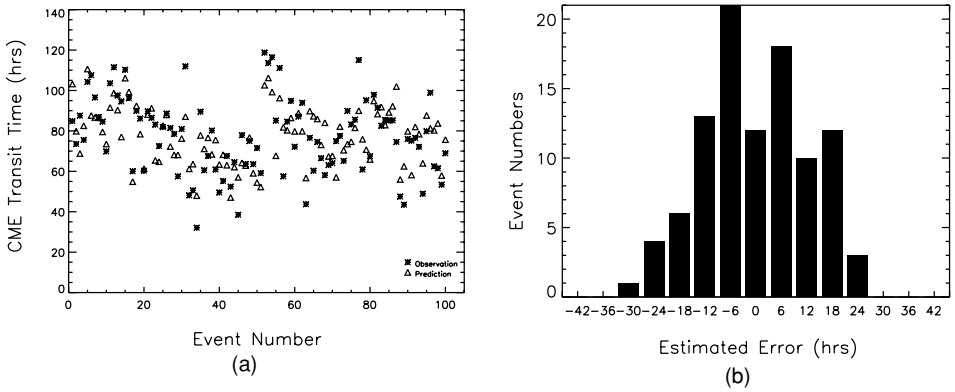

Fig. 9 (a) Comparison between predicted and observed transit times and (b) estimated error of the predictions

in the interplanetary medium need to be investigated in order to further improve predictions of transit times of the Earth directed CMEs and provide reliable indicators for major geomagnetic storms days in advance.

Acknowledgements The work is jointly supported by the National Natural Science Foundation of China (40536029, 40336053, 40374056 and 40523006) and the International Collaboration Research Team Program of the Chinese Academy of Sciences. We are also appreciated for the websites: http://cdaw.gsfc.nasa.gov/CME_list/index.html; ftp:// ftp.ngdc.noaa.gov/ STP/GEOMAGNETIC_DATA/INDICES/ DST/; http: //www.gi. alaska.edu/pipermail/gse-ff/, http:// quake. stanford. edu/wso/ coronal.html for their free data policy.

References

Brueckner, G.E., Delaboudiniere, J.-P., Howard, R.A.: Geophys. Res. Lett. **25**, 3019 (1998)
Burlaga, L.F., Sittler, E., Mariani, F., Schwenn, R.: J. Geophys. Res. **86**, 6673 (1981)
Cane, H.V., Richardson, I.G.: J. Geophys. Res. **108**, 1156 (2003)
Cane, H.V., Richardson, I.G., St. Cyr, O.C.: Geophys. Res. Lett. **27**, 3591 (2000)
Cliver, E.W., Hudson, H.S.: J. Atmos. Sol. Terr. Phys. **64**, 231 (2002)
Crooker, N., Joselyn, J.A., Feynman, J. (eds.): Coronal Mass Ejections, Geophys. Monograph Ser. Vol. 99, AGU, Washington, D. C. (1997)
Crooker, N.U., Siscoe, G.L., Shodhan, S., Webb, D.F., Gosling, J.T., Smith, E.J.: J. Geophys. Res. **98**, 9371 (1993)
Dryer, M.: Space Sci. Rev. **67**, 363 (1994)
Dryer, M., Smart, D.F.: Adv. Space Res. **4**, 291 (1984)
Forbes, T.G.: J. Geophys. Res. **105**, 23153 (2000)
Fry, C.D., Sun, W., Deehr, C.S., Dryer, M., Smith, Z., Akasofu, S.I., Tokumaru, M., Kojima, M.: J. Geophys. Res. **106**, 20985 (2001)
Gopalswamy, N., Lara, A., Lepping, R.P., Kaiser, M.L., Berdichevsky, D., St. Cyr, O.C.: Geophys. Res. Lett. **27**, 145 (2000)
Gopalswamy, N., Lara, A., Yashiro, S., Kaiser, M.L., Howard, R.A.: J. Geophys. Res. **106**, 29207 (2001)
Gosling, J.T.: J. Geophys. Res. **98**, 18937 (1993)
Gosling, J.T., Hildner, E., MacQueen, R.M., Munro, R.H., Poland, A.I., Ross, C.L.: J. Geophys. Res. **79**, 4581 (1974)
Gosling, J.T., McComas, D.J., Phillips, J.L., Bame, S.J.: J. Geophys. Res. **96**, 7831 (1991)
Hakamada, K., Akasofu, S.-I.: Space Sci. Rev. **31**, 3 (1982)
Hudson, H.S., Cliver, E.W.: J. Geophys. Res. **26**, 25199 (2001)
Hundhausen, A.J.: In: Strong, K.T.R., Saba, J.L., Haisch, B.M., Schmelz, J.T. (eds.), The Many Faces of the Sun: A Summary of the Results from NASA's Solar Maximum Mission, p. 143, Springer-Verlag, New York (1999)
Kahler, S.W., Crooker, N.U., Gosling, J.T.: J. Geophys. Res. **104**, 9919 (1999)
Klimchuk, J.A.: In: Song, P., Siscoe, G., Singer, H. (eds.), Space Weather, Geophys. Monograph Ser. Vol. 125, pp.143–157, AGU, Washington D.C. (2000)
Linker, Jon A., Zoran M., Pete R., Roberto L. and Dusan O.: In: Velli, M., Bruno, R., Malara, F. (eds.), Solar Wind Ten, AIP Conf. Proceedings 679, p. 703–710, Melville, New York (2003)
MacQueen, R.M., Csoeke-Poeckh, A., Hildner, E., House, L.L., Reynolds, R., Stanger, A., TePoel, H., Wagner, W.J.: Solar Phys. **65**, 91 (1980)
MacQueen, R.M., Eddy, J.A., Gosling, J.T., Hildner, E., Munro, R.H., Newkirk, G.A., Poland, A.I., Rose, C.L.: Astrophys. J. **187**, L85 (1974)
MacQueen, R.M., Hundhausen, A.J., Conover, C.W.: J. Geophys. Res. **91**, 31 (1986)
Manoharan, P.K., Gopalswamy, N., Yashiro, S., Lara, A., Michalek, G., Howard, R.A.: J. Geophys. Res. **109**, A06109 (2004)
Michalek, G., Gopalswamy, N., Yashiro, S.: Astrophys. J. **584**, 472 (2003)
Moon, Y.J., Dryer, M., Smith, Z., Park, Y.D., Cho, K.S.: Geophys. Res. Lett. **29**, 1390 (2002)
Odstrcil, D., Dryer, M., Smith, Z.: J. Geophys. Res. **101**, 19973 (1996)
Pick, M., Demoulin, P., Maia, D., Plunckett, S.: In: Wilson, A. (ed.), Proc. of 9th European Meeting on Solar Physics: Magnetic Fields and Solar Processes, ESA SP-448, p. 915, Florence, Italy (1999)
Riley, P., Linker, J.A., Mikic, Z., Odstrcil, D.: IEEE Transaction on Plasma Science **32**, 1415 (2004)
Schwenn, R., Dal Lago, Huttunen, E., Gonzalez, W.D.: Annales Geophysicae **23**, 1033 (2005)
Sheeley, N.R., Jr., Howard, R.A., Koomen, M.J., Michels, D.J., Schwenn, R., Mulhauser, K.H., Rosenbouser, H.: J. Geophys. Res. **90**, 163 (1985)
Sheeley, N.R. Jr., Howard, R.A., Michels, D.J., Koomen, M.J.: In: Dryer, M., Tandberg-Hanssen, E. (eds.), Solar and Interplanetary Dynamics., pp. 55–59, D. Reidel, Hingham, Mass (1980)
Shrivastava, P., Singh, N.: Chinese J. Astron. Astrophys. **5**, 198 (2005)
Smart, D.F., Shea, M.A.: J. Geophys. Res. **90**, 183 (1985)
Smith, Z., Dryer, M.: Solar Phys. **129**, 387 (1990)
Smith, Z., Dryer, M.: NOAA Technical Memorandum, ERL/SEL-89 (1995)
Smith, Z., Odstrcil, D., Dryer, M.: J. Geophys. Res. **103**, 20581 (1998)
Srivastava, N., Venkatakrishnan, P.: J. Geophys. Res. **109**, A10103 (2004)
Wang, Y.M., Ye, P.Z., Wang, S.: J. Geophys. Res. **107**, 1340 (2002)

Webb, D.F.: J. Atmos. Sol. Terr. Phys. **62**, 1415 (2000)
Webb, D.F., Cliver, E.W., Crooker, N.U., St. Cyr, O.C., Thompson, B.J.: J. Geophys. Res. **105**, 7491 (2000)
Wei, F.S., Cai, H.C.: Chinese J. Space Sci. **10**, 35 (1990)
Wei, F.S., Cai, H.C., Feng, X.S.: Adv. Space Res. **31**, 1069 (2003)
Wei, F.S., Dryer, M.: Solar Phys. **132**, 373 (1991)
Wei, F.S., Liu, S.Q., Zhang, J.H.: Acta Geophysica Sinica. **34** 133 (1991)
Wei, F.S., Xu, Y., Feng, X.S.: Science in China (E). **45**, 525 (2002)
Wei, F.S., Zhang, J.H., Huang, S.P.: Acta Geophysica Sinica **33**, 125 (1990)
Wilson, R.M., Hilder, E.: Solar Phys. **91**, 169 (1984)
Xie, H., Ofman, L., Lawrence, G.: J. Geophys. Res. **109**, A03109 (2004)
Zhao, X.P., Plunkett, S.P., Liu, W.: J. Geophys. Res. **107**, 10.1029/2001JA009143 (2002)
Zhao, X.P., Webb, D.F.: J. Geophys. Res. **108**, 1234 (2003)